

Facile Tuning of Luminescent Platinum(II) Schiff Base Complexes from Yellow to Near-Infrared: Photophysics, Electrochemistry, Electrochemiluminescence and Theoretical Calculations

Ellen F. Reid,^[a] Vernon C. Cook,^[b] David J. D. Wilson,^[a] and Conor F. Hogan*^[a]

Abstract: The photophysical and related properties of platinum(II) Schiff base complexes can be finely and predictably tuned over a wide range of wavelengths by small and easily implemented changes to ligand structure. A series of such complexes, differing only in the number and positioning of methoxy substituents on the phenoxy ring, were synthesised and their photophysical, electrochemical and electrochemiluminescent (ECL) properties investigated. Theoretical calculations were performed in order to gain further insight into the relationship between structure and properties in these mate-

rials. By positioning methoxy groups *para* and/or *ortho* to either the imine or the oxygen group on the ligand, electron density could be directed selectively toward the LUMO or HOMO as required. This allowed the emission colour (both photoluminescent and electrochemiluminescent) to be tuned over a wide range between 587 and 739 nm. The variation in orbital ener-

gies was also manifested in the positions of the absorption bands and the redox properties of the complexes, as well as in the NMR shifts for the uncoordinated ligands. All reported complexes displayed intense electrochemiluminescence (ECL), which could be initiated either by annihilation or co-reactant pathways. The relationship between the electrochemical and photophysical properties and the efficiency of the ECL is discussed. For two of the complexes solid-state ECL could be generated from electrodeposited layers of the complex.

Keywords: density functional theory • electrochemiluminescence • electrochemistry • luminescence • platinum Schiff base complexes

Introduction

Luminescent transition metal complexes continue to grow in importance due to the diversity of applications for such materials, such as organic light-emitting diodes (OLEDs),^[1] solar cells^[2] and sensors.^[3] Although d⁶ coordination compounds, such as those based on ruthenium and iridium, have been extensively researched, square planar compounds (d⁸ coordination), have received comparatively less attention. Platinum complexes^[4] have received most attention in this class of luminescent materials, with work on these compounds extending back to the 1960s.^[5]

Schiff base ligand systems are attractive because their synthetic chemistry is well developed, making it relatively easy to modify their structure. The synthesis of Schiff-base “salophen” complexes (salophen = *N,N'*-bis(salicylaldehyde)-1,2-phenylenediimino) with metallic centres of ruthenium(II),^[6] chromium(III)^[7] and zinc(II)^[8] have been previously explored. Recently, platinum(II) Schiff base complexes have

been shown to be highly promising candidates for technological applications,^[9] in particular for OLEDs in which their neutral charge, high quantum yields and the stability afforded by the chelate effect make them particularly attractive. The lead compound in the work presented here, platinum(II) salophen (**1**), was first reported in 1991 by Shagisultanova and co-workers.^[10] Che et al.^[11] later reported the properties of a variety of structural variants with a focus on properties related to OLED applications.

In order to gain insight into the structure–function relationship in these and similar materials, we have systematically varied the number and positions of methoxy groups on the phenoxy ring of the salophen ligand, and studied the effects on the photophysical and electrochemical properties of their platinum(II) complexes using a range of experimental and theoretical techniques. We demonstrate that the HOMO and LUMO levels can be independently adjusted through strategic placement of the substituents on the ring.

This study was further motivated by the need for new photoluminescent (PL) and electrochemiluminescent (ECL) sensing materials possessing tuneable emission wavelengths.^[12] Current ECL systems are based almost exclusively on ruthenium polypyridyl systems^[12e] that emit over a limited range, making them unsuitable for multiplexed detection. Furthermore, there is a great need for luminescent sensing materials that emit in the biologically useful near-infrared region. The ECL properties of the systems described here are also of interest in the field of light emitting electro-

[a] Dr. E. F. Reid, Dr. D. J. D. Wilson, Dr. C. F. Hogan
Department of Chemistry, La Trobe Institute for Molecular Science
La Trobe University, Melbourne, Victoria 3086 (Australia)
E-mail: c.hogan@latrobe.edu.au

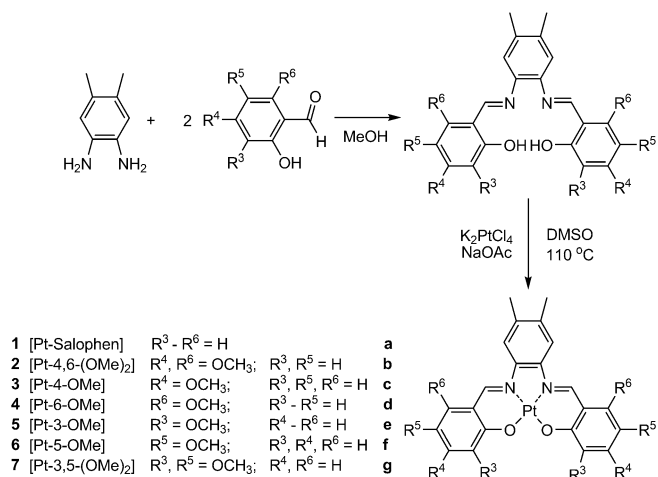
[b] Dr. V. C. Cook
CSIRO, Molecular Health Technologies
Clayton, Victoria (Australia)

Supporting information for this article is available on the WWW under <http://dx.doi.org/10.1002/chem.201302339>.

chemical cells (LECs).^[13] There have been few reported investigations of the ECL of luminescent platinum complexes^[14] and the ECL of platinum(II) Schiff base complexes has not been previously investigated.

Results and Discussion

Synthesis and characterisation: The series of methoxy (OMe) ligands (**a–g**) were synthesised (Scheme 1), with yields varying from 85 to 97% by mixing aromatic diamine



Scheme 1. Synthesis of Schiff base ligands (**a–g**) and platinum(II) complexes (**1–7**).

with the corresponding aldehyde in methanol. In the original report of the synthesis of the lead complex **1** by Shagisultanova and co-workers,^[10b] aqueous tetrachloroplatinate was mixed with a KOH ligand solution in aqueous acetone.^[10a] However, this method gives a low variable yield producing large amounts of colloidal platinum. Moreover, the solubility of the product appears to be dependent on the purity, which can make subsequent separations difficult. The present work employs the method that was reported by Lu et al.^[15] using a mixture of DMF and DMSO and the softer base sodium acetate.

The pure Schiff base platinum complexes are rather insoluble in common solvents, such as methanol and acetonitrile. Unreacted ligand increases the solubility of the complexes making column chromatography and simpler recrystallisation techniques difficult. These issues can be overcome by using a slight excess of platinum in the reaction. Complexes **1–7** were synthesised by adding potassium tetrachloroplatinate to a hot solution of DMSO, sodium acetate and the respective ligand (Scheme 1). This allows virtually all the ligand to be reacted and converted in the respective complexes, leaving unreacted platinum and other salts as by-products in solution. The platinum complexes are either crystallised from the reaction mixture or precipitated with

a little water. The product is filtered off and washed with excess solvent. Yields for complexes varied from 65 to 85%.

The ¹H NMR spectra of the unbound ligands are relatively straightforward, with all but the aromatic regions of ligand **b** and **c** being clearly resolved. Of particular note are the phenolic OH resonances, which are all clearly resolved in CDCl₃ and significantly shifted down-field due to interactions with the imine group. This OH proton is effectively coordinated between the phenolic oxygen and the imine nitrogen. The position of this peak is strongly influenced by the positioning of the methoxy groups on the adjacent phenyl ring (Figure S1 in the Supporting Information). In ligand **b**, **c** and **d** in which the ring is substituted at one or both positions *meta* to the phenoxy oxygen (R⁴ and R⁶), the peak is shifted down-field relative to **a**. Similarly, for **e**, **f** and **g** there is a general up-field shift in this peak with substitution at the positions *ortho* and/or *para* to the oxygen group (R³ and R⁵). This variation in deshielding effect is mirrored in the photophysical and electrochemical properties of complexes prepared from these ligands, as discussed in the next section. The substitutions have less effect on the HC=N imine proton resonance with the exception that the presence of a methoxy in the R⁶ position shifts the resonance down-field. This is most likely due to interactions with the oxygen lone pairs.

In the platinum complexes the imine proton is moved down-field to at least 9.19 ppm. This peak has a reduced integration and a pair of broad satellites due to three-bond coupling to the 34% naturally abundant ¹⁹⁵Pt isotope. The aromatic protons of the complexes are more clearly resolved than in the aromatic protons in the free ligands.

Photophysical properties: The spectroscopic properties of all complexes are summarised in Table 1. The UV/Vis absorption spectra in dichloromethane of **1**, **2** and **5** are depicted in Figure 1. The bands in the high-energy region of the absorption spectrum (<350 nm) can be attributed to ligand based (π–π*) transitions. Each complex contains one intense absorption peak at about 260 nm, close to where the free ligand is found to absorb strongly.^[16] Between 350 and 400 nm, two or three absorption bands for each of the complexes are observed. These bands can be attributed to a mix-

Table 1. Photoluminescence and absorbance spectroscopic data for dilute solution of **1–7** in CH₂Cl₂.

Complex	λ _{em} [nm] ^[a]	E _s [eV] ^[b]	Φ _{em} [%]	λ _{abs} [nm]
1	620	2.00	3.8	534, 498, 463, 381, 362, 321, 252
2	587	2.11	1.6	496, 401, 381, 361, 254
3	590	2.10	5.6	505, 475, 441, 381, 365, 315, 254
4	615	2.02	4.9	526, 505, 461, 407, 384, 334, 254
5	647	1.91	3.5	538, 516, 468, 395, 373, 351, 263
6	698	1.78	4.8	575, 545, 498, 387, 366, 322, 263
7	739	1.68	0.6	581, 548, 508, 396, 370, 335, 254
[Ru(bpy) ₃] ²⁺	620	2.00	2.7	450, 270

[a] Responses corrected for variation in detector sensitivity with wavelength; [b] E_s = hc/λ, in which h is the Planck constant [eVs], c is the speed of light and λ is the wavelength of emission.

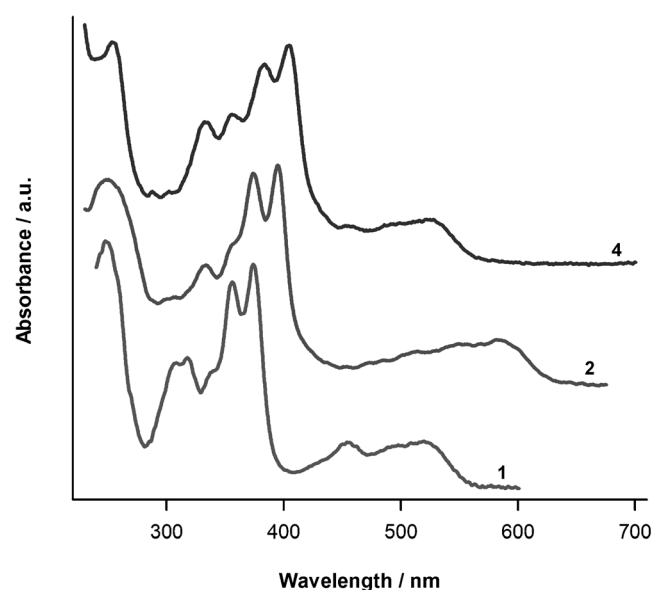


Figure 1. Absorption spectra of **1**, **2** and **4** in CH_2Cl_2 at 298 K (spectra offset for clarity).

ture of metal-to-ligand $[\text{Pt}^{\text{II}} \rightarrow \pi^*(\text{L})]$ and intraligand $[\text{L}(\text{phenoxide}) \rightarrow \pi^*(\text{imine})]$ charge transitions.^[17] All complexes exhibit three moderately intense absorption bands in the 440–600 nm range. These are attributed to the metal-to-ligand-charge-transfer (MLCT) processes; formally, one electron from each of the metal orbitals (b_{2g} -, e_g - and a_{1g} -) moves into the anti-bonding π^* orbital of the salophen²⁻ ligand. Similar observations have been made by Shagisultanova et al.^[10b] and Che et al.^[11a,b] for these types of complexes. There is a strong trend in the absorbance data across the methoxy-salophen series, with the MLCT absorbance bands progressively shifting from 496 to 581 nm on going from **2** to **7**. Note that **2**, **3** and **4** are blue-shifted with respect to **1** whereas **4**, **5** and **6** are red-shifted. This is consistent with increasing electron donating ability towards the phenoxy group and metal centre for **5**, **6** and **7**, and toward the imine in the case of **2**, **3** and **4**. This will be discussed further in the calculations section.

All complexes are luminescent in anaerobic CH_2Cl_2 solution at 298 K and display structured emission profiles (Figure 2). In general, the complexes showed moderately high photoluminescence quantum yields (ϕ_{em}); for example, all but two are more luminescent than $\text{Ru}(\text{bpy})_3^{2+}$ under identical experimental conditions.

The phosphorescence in these complexes originates from the transitions between the lowest triplet excited state, which has mixed $[\text{L}(\text{phenoxide}) \rightarrow \pi^*(\text{imine})]$ and $[\text{Pt}(\text{5d}) \rightarrow \pi^*(\text{Schiff-base})]$ charge-transfer character, and the singlet ground state.^[11c] Hence, the emissive excited state does not originate purely from a metal-to-ligand transition.^[11,18] Complexes **1–4** each exhibit three distinct peak maxima in their photoluminescence spectra, with an average vibronic progression^[11a,17] of 1470 cm^{-1} . For example, complex **1** has peak maxima at 587, 642 and 710 nm (vibronic progres-

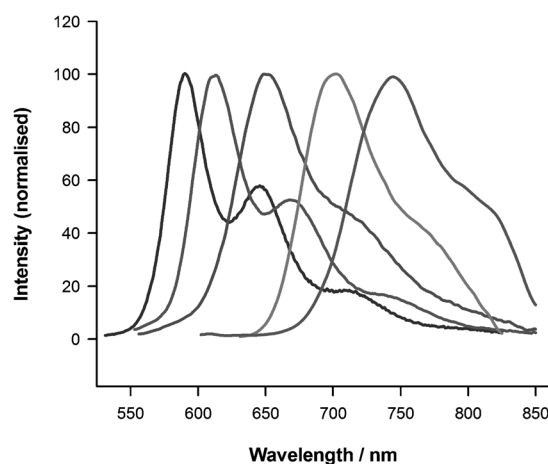


Figure 2. Photoluminescence spectra for (from left to right) complexes **2**, **4**, **5**, **6** and **7** in CH_2Cl_2 at 298 K. The spectral profiles have been corrected for variation in detector sensitivity with wavelength.

sions = 1460 and 1490 cm^{-1}). Complexes **5–7** show a less distinct shoulder that is red-shifted by approximately 75 nm from the primary emission peak. These observations are consistent with an intraligand component to the excited state and are similar to the conclusions of Che et al.^[11b] for tetradentate Schiff-base platinum complexes, similar in structure to **1**.

The emission maxima (λ_{em}) of the complexes increase in the order $2 < 3 < 4 < 1 < 5 < 6 < 7$. Similar to the trend observed for the absorbance data, the emission colour is red-shifted or blue-shifted with respect to **1** depending on the positions of the methoxy substituents on the bonded ligand. This trend can be very satisfactorily explained in terms of the extent to which electron density is directed toward the HOMO or LUMO, as dictated by the positions of the methoxy substituents. For example, **2**, **3** and **4** are substituted at positions *ortho* and/or *para* to the imine group (R^6 and R^4) and the emission energy increases according to the following pattern: *ortho* < *para* < *ortho* and *para*. This is consistent with a LUMO residing substantially on the imine moiety, which is progressively destabilised on going from **4** to **3** to **2**. A similar argument applies to complexes **5**, **6** and **7**, which are substituted at positions R^3 and R^5 , *ortho* and/or *para* to the metal bonded oxygen. In this case the HOMO is progressively destabilised on going from **5** to **6** to **7**, which has the effect of decreasing the size of the HOMO–LUMO gap and lowering the energy of the emission. This will be elaborated on in the calculation section.

Electrochemical properties: The electrochemical data for complexes **1–7** are summarised in Table 2. The cyclic voltammetric responses for **1**, **3** and **4** in CH_2Cl_2 at 298 K are depicted in Figure 3. Complexes **1–4** all show a similar quasi-reversible oxidation pattern with the forward wave in the range of $E_{\text{pa}} = 0.45$ to 0.73 V versus $[\text{Cp}_2\text{Fe}]^{+/0}$ and the reverse peak in the range of $E_{\text{pc}} = 0.27$ to 0.52 V versus $[\text{Cp}_2\text{Fe}]^{+/0}$. Complexes **6** and **7** show similar quasi-reversible wave patterns with the forward wave at $E_{\text{pa}} = 0.35$ and

Table 2. Electrochemical data for **1–7** at 298 K in CH₂Cl₂ with 0.1 M TBAPF₆ supporting electrolyte.

Complex	Potential [V] (vs. Fc) ^[a]				$E_{\text{pa}}(\text{I}) - E_{\text{pc}}(\text{II})$ [V] (HOMO–LUMO) ^[b] [eV]
	oxidative process (I)		reductive processes (II)		
	E_{pa}	E_{pc}	E_{pc}	E_{pa}	
1	0.73	0.30	–1.98	–1.20	2.72
2	0.45	0.27	–2.11	–1.17	2.58
3	0.63	0.36	–2.05	–1.15	2.68
4	0.68	0.52	–1.97	–1.07	2.64
5	0.35	0.19	–1.80	–	2.18
6	0.46	0.22	–1.75	–0.98	2.33
7	0.53	0.33	–1.83	–	2.28

[a] $E_{1/2}$ ferrocene (Fc) was 0.35 V versus Ag/AgCl; [b] the values for the electrochemical HOMO–LUMO gap are numerically the same as the values for ΔG_{ann} for the annihilation reaction between the oxidised and reduced species as discussed later.

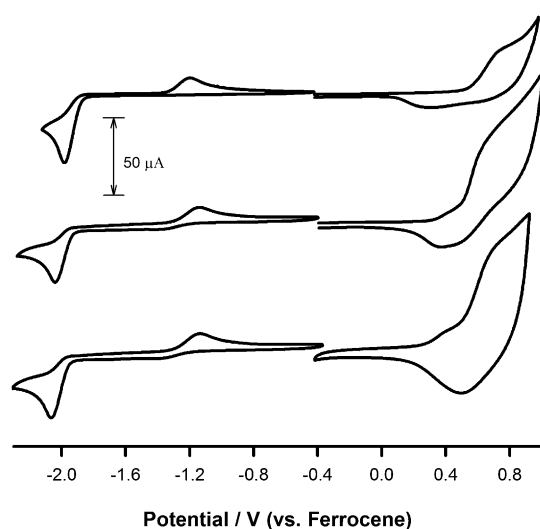


Figure 3. Cyclic voltammograms for 1 mM solutions of **1** (top), **3** (middle) and **4** (bottom) in CH₂Cl₂, 0.2 V s^{–1} scan-rate, 0.1 M TBAPF₆ supporting electrolyte.

0.53 V and the reverse peak at $E_{\text{pc}} = 0.19$ and 0.33 V, respectively. Complex **5** shows an irreversible oxidation wave at $E_{\text{pa}} = 0.68$ V. Controlled potential coulometry was performed to determine the number of electrons transferred per molecule for the anodic wave observed in the cyclic voltammogram. When bulk electrolysis was performed at potentials 200–300 mV less positive than $E_{1/2}$, no electrons were counted. When the potential of electrolysis was set 200 mV more positive than $E_{1/2}$, two electrons were found to be transferred per molecule based on the charge passed per mole of complex. Thus the quasi-reversible oxidation processes can be formally attributed to the Pt²⁺/Pt⁴⁺ couple in each case. The reductive pattern is similar for each complex, with an irreversible peak observed on the negative going scan and an associated anodic peak at more positive potentials on the return scan (except for **5** and **7**, which did not display an anodic peak on the return scan). These irreversible reductions are presumed to be ligand centred.

Similar to the photophysical properties discussed above, noticeable trends are apparent between the electrochemical properties and the charge donating characteristics of the ligand as determined by the placement of the methoxy substituents. The electrochemical data presented in Table 2 indicate that complexes **4**, **3** and **2** become progressively more difficult to reduce as more electron density is directed toward the imine moieties whereas the reduction potentials for **5**, **6** and **7** are relatively invariant. Although the trend in the oxidation data is less obvious, it is clear that the red-shifted complexes are oxidised at lower potentials than the corresponding blue-shifted complexes. The HOMO–LUMO gap may be estimated by the difference in the ground state redox potentials.^[19] The results in Table 2 further indicate that there is a similar trend between the electrochemically estimated “gap” and the energy corresponding to the emission maxima. In general, although the quasi-reversible nature of the electron transfer processes complicates their interpretation, the electrochemical data suggest that the optical and electrochemical properties of these complexes are similarly tuned by varying the ligand structure.

Spectroelectrochemistry: To probe the nature of the oxidised species spectroelectrochemical measurements were performed. Figure 4 shows the changes in the visible absorp-

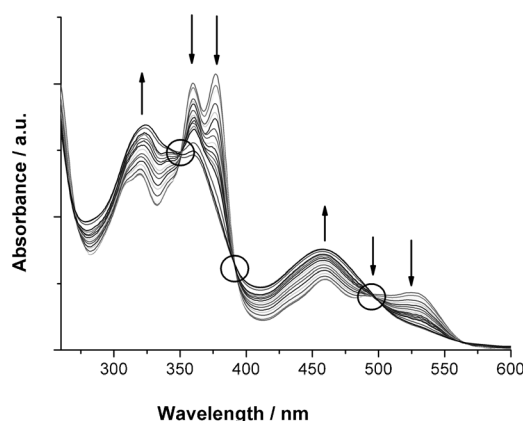


Figure 4. Changes in UV–visible absorbance spectrum during electrolysis of 0.5 mM solution of **1** in CH₂Cl₂/0.1 M TBAPF₆. The potential of the Pt gauze electrode was held at constant potential of 1.0 V versus Fc. during the course of the oxidation.

tion spectrum while electrochemically oxidising a 0.5 mM solution of complex **1**. The potential was maintained at 1.00 V versus ferrocene (≈ 250 mV more positive than E_{p}) and a spectrum acquired every 30 s until no further spectroscopic changes were observed. Three clear isosbestic points at 493, 392 and 352 nm are apparent indicating that no intermediate products are generated during the electrolysis. The observed spectral changes due to the oxidative process are fully reversible with the original species easily regenerated through bulk electrolysis at a potential more negative than the oxidation peak. Several absorbance bands are completely lost during the electrolysis from both the MLCT region

(498 and 534 nm) and intraligand charge transfer region (381 nm). This suggests that the HOMO has both metallic and ligand characteristics. The complete loss of two of the three MLCT bands suggests this process to be primarily localised on the platinum centre. Che et al.^[11b] reported similar Schiff-base platinum complexes to have an emissive triplet excited state with mixed MLCT and ILCT characteristics. These observations are also consistent with the theoretical calculations presented later.

Electrogenerated chemiluminescence (ECL): Annihilation ECL was observed for all the complexes by pulsing the potential of the working electrode sequentially past the oxidation and then the reduction potential of the complex. The generation of the excited state, $[\text{Pt}^{\text{II}}\text{salophen}]^{2+*}$ via annihilation ECL involves electron transfer reaction between the oxidised and reduced forms of the species.^[20] In the present case, the mechanism is assumed to involve two sequential electron transfers [Eq. (3) and (4)], the second of which results in formation of the excited state product.^[21]



In order to determine whether annihilation ECL is possible, the free energy available from the electron transfer reaction between the oxidised and reduced species (ΔG_{ann}) can be estimated from the electrochemical data (Table 3) using the following relationship (entropic contributions neglected):

$$-\Delta G_{\text{ann}} = E_{\text{pd}}(\text{I}) - E_{\text{pc}}(\text{II}) \quad (6)$$

This may be compared with E_s , the energy of the excited state (Table 1). Taking complex **1** as an example, $-\Delta G_{\text{ann}}$ (2.72 eV) is in excess of the energy required to populate the

Table 3. Electrochemiluminescence (ECL) data.

Complex	λ_{ECL} [nm]	Relative ECL intensity	
		ECL _{ann} ^[a]	ECL _{TPrA} ^[b]
1	620	489.6	0.1
2	595	229.0	0.2
3	591	73.5	1.0
4	615	0.6	2.0
5	646	0.6	49.5
6	696	1.0	35.6
7	739	3.9	1.9
$[\text{Ru}(\text{bpy})_3]^{2+}$	620	100.0	100.0

[a] Annihilation ECL integrated intensities corrected for charge passed during forward step and compared to the same experiment with $[\text{Ru}(\text{bpy})_3]^{2+}$ in CH_2Cl_2 ; [b] co-reactant ECL compared to $[\text{Ru}(\text{bpy})_3]^{2+}$ /TPrA in CH_2Cl_2 .

excited state, E_s (~2.00 eV) therefore ECL is possible. Similarly it can be shown that all of these $\text{Pt}^{\text{II}}\text{salophen}$ systems are energy sufficient annihilation ECL systems.^[22]

As shown by the data in Table 3, the most intense ECL emitter, under annihilation conditions is complex **1**, followed closely by **2** and **3**. Complexes **1** and **2** give ECL intensities, which are significantly more intense than the benchmark ECL emitter, $[\text{Ru}(\text{bpy})_3]^{2+}$, tested under the same conditions. Although these three complexes have the most negative reduction potentials of all the complexes, there is no obvious correlation between annihilation reaction exergonicity and ECL intensity as might be expected from Marcus theory.^[23,24] Moreover, all of the annihilation reactions are energy sufficient for ECL by at least 0.27 eV. It may be surmised therefore, that a large ΔG_{ann} is a necessary but not sufficient condition for intense ECL.

Co-reactant ECL was also observed for all complexes in the presence of tripropylamine (TPrA) with light emission occurring in each case, at the potential corresponding to the oxidation of the platinum complex (Figure 5). The co-reactant (TPrA) is oxidised in the same potential step as the Pt^{2+} species, the oxidised TPrA then generates a product that reacts with Pt^{4+} to generate the excited state, which subsequently produces light.

The mechanism, outlined below is based on the ECL experiments of $[\text{Ru}(\text{bpy})_3]^{2+}$ /TPrA^[25] and other transition

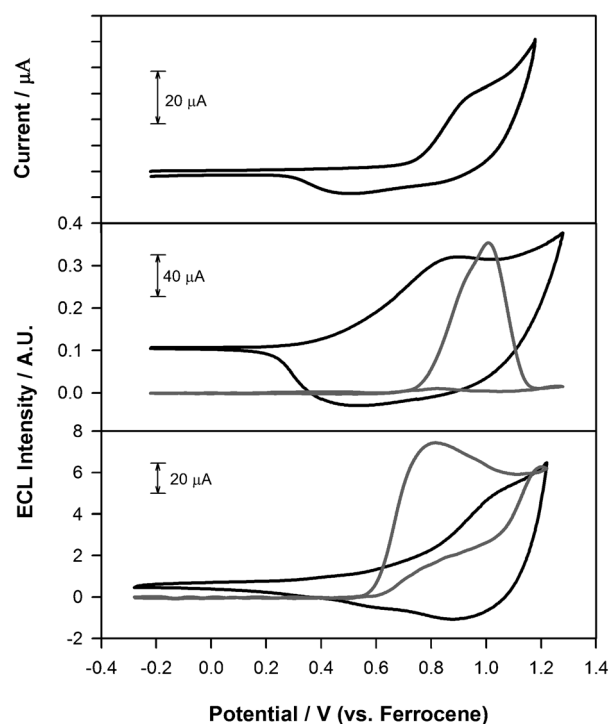
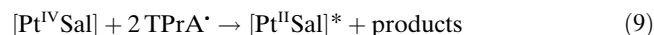


Figure 5. Complex **1** (1 mM) in CH_2Cl_2 , 0.1 M TBAPF₆ supporting electrolyte, 0.2 Vs^{-1} scan-rate. Top: solution phase response in the absence of co-reactant. Middle: solution phase cyclic voltammetric (black) and ECL (grey) response in the presence 1 mM TPrA co-reactant. Bottom: solid-state cyclic voltammetric (black) and ECL (grey) response in the presence of 1 mM TPrA co-reactant.

metal/TPrA systems, except that two presumably sequential reductions [Eq. (9)] are required:



The most intense ECL emitter under co-reactant conditions is complex **5**, followed closely by **6**. This appears to be the inverse of the case with the annihilation ECL intensities, as these two complexes have the least negative reduction potentials. As pointed out by Lee et al.^[26] an important requirement for efficient co-reactant ECL is that the reduction potential for the reductant (TPrA[·] in this case) be more negative than the reduction potential (~LUMO energy level) for the complex. This is of course necessary in order for the reaction in Equation (9) to be energy sufficient. Given that $E^\circ(\text{TPA}^{\cdot})$ is approximately -2.1 V versus ferrocene,^[27] it can readily be understood from the reduction potential data in Table 2 why complexes **5** and **6**, which have the least negative potentials, produce more intense co-reactant ECL relative to the other complexes.

There is also a relationship between the oxidation potential for the complex and ECL intensity, with the two most intense emitters having the lowest oxidation $E_{1/2}$. This may be explained by the fact that more easily oxidised species are much less likely to undergo parasitic side reactions, which degrade ECL efficiencies, while noting that the oxidation potential of the complex is still positive enough to effectively oxidise TPrA in each case.

Another important determinant of ECL efficiency is photoluminescence quantum yield, since this represents the upper limit of efficiency for the overall ECL process. However, no correlation is observed between the PL and ECL efficiencies of the complexes. This and the previous observations highlight the complexity of ECL systems and the difficulty associated with predicting ECL ability on the basis of electrochemical or spectroscopic characteristics, as pointed out by other workers.^[20a,28]

Figure 6 shows the ECL spectra for complexes **1**, **2**, **5** and **6** obtained using the co-reactant method. Emission maxima (Table 3) were found to closely match the photoluminescence spectra; therefore, the same excited state is populated regardless of whether optical or electrochemical excitation is employed. Minor differences in shape between the ECL and PL spectra are due to differences in instrument resolution and concentration effects.

An interesting and potentially useful aspect of the electrochemical properties of some of the complexes studied here is illustrated in Figures S2–S5 in the Supporting Information. These figures show the consistent growth in anodic current, which occurs upon successive scanning of complexes **1** and **3** at concentrations > 1 mM. The growth in the current stabilis-

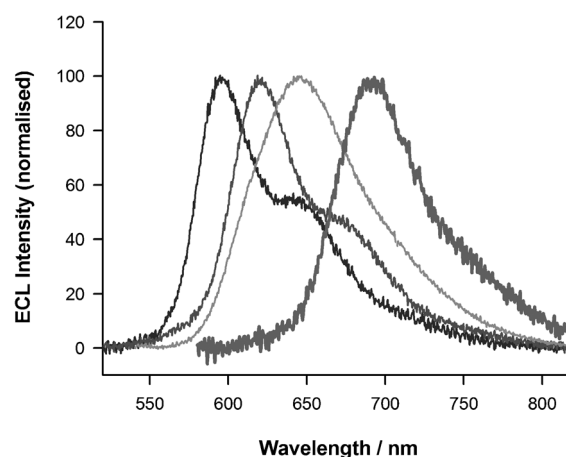


Figure 6. ECL spectra for 1 mM solutions of complexes (left to right) **2**, **1**, **5** and **6** in CH_2Cl_2 containing 0.1 M TBAPF₆ as supporting electrolyte and 10 mM TPrA co-reactant.

es after approximately 10 scans. Under these conditions the formation of an insoluble film at the surface of the glassy-carbon working electrode is observed. The electrochemical properties of the insoluble film are conserved when transferred into blank dichloromethane/electrolyte solution. Peaks associated with the oxidation and reduction of the film were also observed in aqueous systems of either phosphate buffer (pH 7.0) or sulfuric acid (0.1 M). The film was stable for in excess of 50 repetitive scan cycles in either aqueous or organic media. The film formation for **1** was suggested by Shagisultanova et al.^[10b] to be due to the generation of a polymeric or partially oxidised species in which the partially vacant d orbital of the oxidised metal may accept a π electron from the phenyl rings of the salophen ligand of a neighbouring molecule. As shown in Figure 5c, ECL activity was also observed for the film in organic media. When the modified electrode was electrochemically cycled in the presence of TPrA as co-reactant, emission was detected at the potential corresponding to the oxidation of the solid. Spectral analysis of the luminescence (Figure S4 in the Supporting Information) showed that it was slightly red-shifted compared to the emission produced by the complex in solution. The ability to electrodeposit these materials while conserving their properties may be useful for technological applications.

Theoretical calculations: The TD-DFT results generally support the assignment of absorption bands from the experimental data. The assignment of transitions as being either pure MLCT or ILCT would not be justified due to the delocalisation of the MOs, and in particular the HOMO, of these complexes. Moreover, the presence of spin-orbit coupling in heavy metal complexes such as these further obfuscates the separation between singlet and triplet states, as well as CT states. The absorption bands at lower energy (above 400 nm) are generally associated with a greater degree of MLCT, although inclusion of spin-orbit coupling would be required to accurately model this region of the spectrum.

The influence of the substituents on the aromatic ligand system may be rationalised in terms of mesomeric (resonance) and inductive effects. The mesomeric effect is directly related to the sharing of π electrons between the aromatic core and the substituent, which is influenced by the topology of electron density of the relevant MO. If the substituent is attached in a position of little electron density, such as at a node, or where the coefficient of the linear combination of atomic orbitals (LCAO) is small, then the effect of the substituent on the MO will be weak. Conversely, if the attachment is at a point of significant electron density, then the interaction will be stronger and the MO more readily effected. For a methoxy substituent the mesomeric effect is dominant over inductive effects, and so the following discussion is based on mesomeric effects.

Substituent effects have been examined by comparing the electron density of each complex with the unsubstituted complex, **1**. The nature of the substituent has a small, yet important effect on the energy and nature of the frontier MOs of the complexes. Similar topologies were found for the HOMO and LUMO of each platinum complex **1–7**. The HOMO and LUMO for **1** are illustrated in Figure 7, with

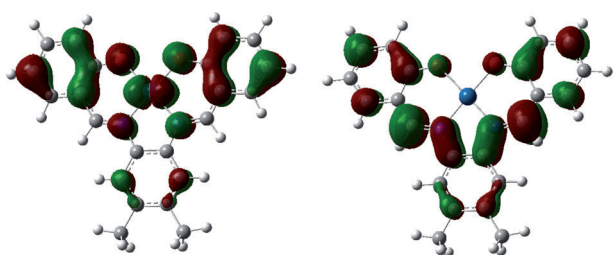


Figure 7. Isodensity surfaces of the HOMO (left) and LUMO (right) of complex **1**. Calculated at the mPW1PW91/SDD, TZVP level of theory inclusive of CH_2Cl_2 solvation effects (SCRFF, IEFPCM).

MOs of the remaining complexes included in the Supporting Information (Figure S6). In all complexes the HOMO is not purely metal-based but delocalised over the complex. This is consistent with results from the spectroelectrochemistry experiments, which suggested that the HOMO has both metallic and ligand character. A notable trend is that the platinum contribution to the HOMO is greater in complexes **1–4** (22–24%) than for **5–7** (10–15%). For all complexes, the LUMO is entirely ligand based, with less than 0.2% contribution from the metal. Fragment contributions to frontier MOs are plotted in Figure S7 in the Supporting Information.

Two factors are critical to understanding the observed trends in photophysical properties of the seven complexes. Firstly, the HOMO of all complexes contains almost zero contribution from carbon atoms at R^3 and R^5 (LCAO is zero; a node passes through these positions) but contains a significant contribution from carbon atoms at R^4 and R^6 (significant electron density is present at these positions). The reverse is observed in the LUMO of all complexes. This is illustrated in Figure 7 for the case of complex **1** (Figure S6 in the Supporting Information for complexes **2–7**). Secondly,

the substituent methoxy-phenol ring interaction is in all cases antibonding with respect to the C–O(Me) bond.

On this basis, it is possible to predict methoxy substituent effects in these complexes (in comparison with complex **1**). Substitution at the R^4 and/or R^6 positions will impact the energy of the HOMO much more than the LUMO, and substitution at the R^3 and/or R^5 positions will have a greater impact on the energy of the LUMO over the HOMO.

For complexes **5–7**, methoxy substitution occurs at R^4 and/or R^6 (*ortho* and *para* to the platinum-coordinated oxygen). At both the R^4 and R^6 positions in the aromatic ring there is significant contribution to the electron density in the HOMO (non-zero LCAO) and so substituent mesomeric effects will be significant. Since the C–O(Me) interaction is actually antibonding, the HOMO is destabilised relative to complex **1**, as is observed in the MO energies plotted in Figure 8. For complexes **2–4**, methoxy substitution occurs at R^3 and/or R^5 (*meta* to the platinum-coordinated oxygen), where there is little electron density (a node with LCAO coefficients almost zero). Since there is little contribution to the HOMO from the ring carbons at R^3 and R^5 , the mesomeric effect is weak and the HOMO energy for **2–4** may be expected to be similar to that of **1**, which is noted in Figure 8.

An analogous trend is noted for the LUMO of these complexes, which contain a significant contribution (non-zero

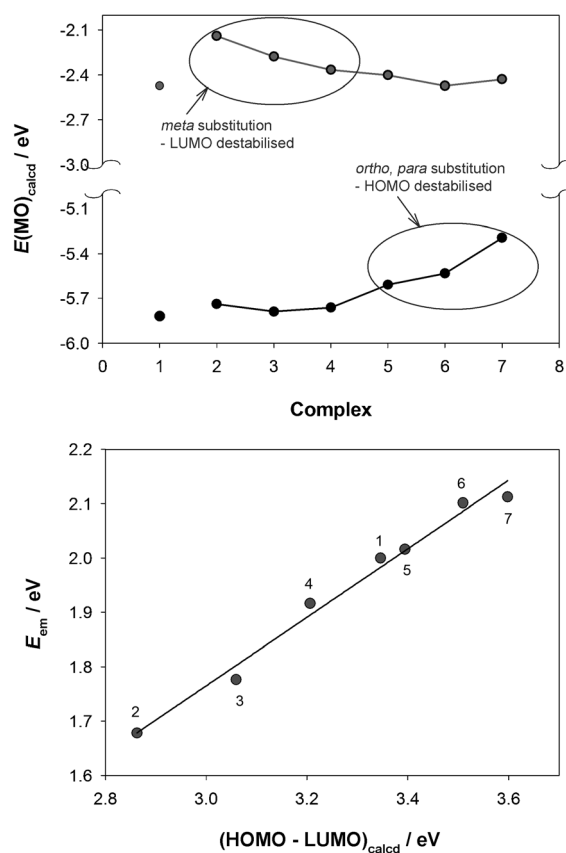


Figure 8. Plot of HOMO/LUMO energies (top) and correlation between calculated HOMO–LUMO gap and emission energy (E_{em}).

LCAO coefficients) from the ring carbon atoms at the R⁴ and R⁶ positions. For complexes **2–4**, methoxy substitution at R⁴ and/or R⁶ will significantly affect the energy of the LUMO, which is substantially localised on the imine group. Since the C–O(Me) interaction is antibonding, substitution at R⁴ and R⁶ will destabilise the LUMO energy relative to complex **1**. For complexes **5–7**, substitution at R³ and/or R⁵ (where there is little electron density) does not have a substantial mesomeric effect, and so the energy of the LUMO remains similar to that of **1**.

To confirm this analysis, calculations were performed for hypothetical complexes, **2Me**, **7Me**, **2CN** and **7CN**, similar in structure to **2** and **7** but with CN and methyl substituents replacing OMe. The dominant electron donating/withdrawing effects are: OMe is a mesomeric electron-donor and is *ortho/para* directing, Me is an inductive electron-donor and is *ortho/para* directing, and CN is a mesomeric electron-withdrawing group and is *meta* directing.

If we first compare the electron-donating and *ortho/para* directing OMe and Me groups, it is noted that the HOMO–LUMO gap of **2Me** is greater than that of **7Me**; however, the effect on the HOMO–LUMO gap is much less for Me (inductive e-donor) than for OMe (mesomeric e-donor). Since resonance effects are not significant for Me (as with OMe), destabilisation of the LUMO of **2** and the HOMO of **7** will not occur to the same extent as is calculated for OMe. In fact, for **2Me** the substituent effect (relative to **1**) is greater for the HOMO rather than the LUMO, which results in the HOMO–LUMO gap of **2Me** being smaller than that of **1**.

With the *meta*-directing CN substituents, which are predominantly mesomeric electron-withdrawing, the effects on the HOMO and LUMO energies are quite substantial and are opposite in effect to the OMe substituents. That is, the HOMO–LUMO gap for **2CN** is approximately equal to that of **7** (less than for **1**), whereas the energy gap for **7CN** is similar to that of **2** (greater than for **1**). This is to be expected, as substitution at R⁴/R⁶ for the *meta*-directing CN group will mostly impact the LUMO energy, whereas substitution at R³/R⁵ will impact the HOMO energy (opposite to that of OMe).

These results confirm our analysis, that by changing substituents we can modify the energies of the HOMO and LUMO orbitals and thus serve to “fine-tune” the HOMO–LUMO gap. With an understanding of substituent mesomeric and inductive effects and frontier MOs of the metal–ligand complex, emission colour tuning may be achieved. This “tuning” is reflected in the electrochemical and photophysical measurements.

Conclusion

The emission colour and other properties of platinum(II) salophen complexes may be readily and predictably tuned over a wide range by small, easily implemented variations to the ligand structure. By methodically varying the positions

of OMe substituents on the phenoxy ring of the salophen ligand in a series of seven complexes, we have demonstrated the ability to systematically and independently modulate the energies of the HOMO or the LUMO in these systems. Because OMe is electron-donating and *ortho/para* directing it can be used to destabilise the imine-localised LUMO by placement at positions R³ and/or R⁵, whilst having virtually no impact on the HOMO. Similarly, placement at positions R⁶/R⁴, *ortho/para* to the Pt–O localised HOMO, destabilises this orbital without impacting on the LUMO. The facility to independently tune the HOMO and LUMO is desirable for a variety of reasons, for example the need to modulate emission colour while maintaining constant oxidising power in ECL-based sensing.

DFT calculations are in very satisfactory agreement with the experimental photophysical results and strongly support the interpretation of the data. Furthermore, calculations show the feasibility of employing other substituents with different properties to modulate the properties of the complexes in differing ways. For example, the *meta*-directing, mesomeric electron withdrawing CN group will have an effect equal but opposite to OMe, whereas a methyl group, which is an inductive rather than mesomeric electron-donor, will direct electron density in a similar way to OMe but with smaller effect. Obviously, the effect could also be amplified by choosing a stronger mesomeric electron withdrawing substituent, such as NH₂, allowing the colour to be tuned over an even wider range of wavelengths.

The electrochemical properties of the complexes in general mirror the photophysical results, with the redox levels being tuned in a similar way. However, the quasi-reversible nature of the redox processes tends to obscure the correlation. This is the first report of ECL from Pt^{II} Schiff base complexes; all of the complexes show intense ECL through both annihilation and co-reactant pathways. Complexes **6** and **7** are of particular note because near-infrared emitting electrochemiluminophores are rare. The determinants of ECL efficiency are found to be complex and interrelated and different factors appear to dictate the efficiency of annihilation and co-reactant ECL. In most cases the ECL intensity for the compounds reported here does not exceed that of the Ru(bpy)₃²⁺ standard, however, the ability to tune the colour of the electrogenerated emission is unsurpassed in ECL systems.

Experimental Section

Instrumentation and apparatus: The electrochemical measurements were carried out using an Eco Chemi μ -Autolab type II potentiostat or a CH instrument model 660B electrochemical workstation. Electrochemiluminescence (ECL) experiments were performed using the μ -Autolab with a custom built light-tight Faraday cage and a photomultiplier tube (Electron tubes Ltd., model 98285B), biased at 600 V, which was coupled to a transimpedance amplifier (AMES). All solution-phase electrochemical experiments were performed in a quartz bottomed cell. The working electrode was a 3 mm in diameter glassy carbon (GC) disk electrode (CH Instruments), the counter electrode a platinum wire and the reference

electrode was a nonaqueous silver wire electrode (CH Inst; blank electrolyte filling solution) for organic media. A silver/silver chloride reference electrode (filling solution; 3 M KCl) was used for aqueous systems.

Experiments conducted in organic media were referenced to the formal potential of the ferrocene/ferrocenium couple measured in situ for each complex. Electrochemical experiments in organic media were performed in 0.1 M tetra-*n*-butylammonium hexafluorophosphate (TBAPF₆; electrochemical grade) in anhydrous dichloromethane (>99.8% with amylene stabiliser) with a complex concentration of 1.0×10^{-3} M. Aqueous solutions were prepared using deionised water ($18 \text{ M}\Omega \text{ cm}^{-1}$). All scans were conducted at 0.2 V s^{-1} unless otherwise stated and carried out at ambient temperatures ($20 \pm 2^\circ \text{C}$). All solutions were deoxygenated using grade 5 nitrogen prior to electrochemical experimentation. The GC working electrodes were polished prior to each experiment using BUEHLER Micro-cloth® Polishing cloth with an aqueous slurry of $0.3 \mu\text{m}$ alumina.

Spectro-electrochemical measurements were performed using Varian Cary UV/Vis spectrometer and a CH660B potentiostat with a 1 mm path-length thin layer quartz spectroelectrochemical cell. A platinum gauze working electrode, platinum wire counter electrode and silver wire reference electrode was employed. Bulk electrolysis (coulometric) experiments were performed in a 20 cm^3 cell using a platinum gauze working electrode, silver wire reference and a platinum counter electrode separated from the main solution via a porous frit. The solution was stirred (magnetic stirrer) during electrolysis.

NMR spectra were obtained with a Bruker BioSpin Av200 with an operating frequency of 200.13 MHz. Accurate mass electrospray mass spectra were recorded with a Micromass Q-TOF II mass spectrometer using a cone voltage of 50 V and a capillary voltage of 3.0 kV. ECL spectra were obtained using a QE65000 Scientific-grade Spectrometer, incorporating a Hamamatsu S7031-1006 FFT-CCD detector. UV/Vis spectra were recorded using a Varian Cary UV/Vis spectrometer with Eclipse software. Emission spectra at ambient temperature were obtained on a Varian Cary Eclipse fluorescence spectrometer and were corrected. All solutions for photophysical measurements used a 10 mm path-length sealable quartz cell and were degassed with nitrogen (15 min) prior to experimentation.

Emission quantum yields were determined using either the single point (3–7) or multiple-point (1 and 2) method. A degassed dichloromethane solution of $[\text{Ru}(\text{bpy})_3]\text{PF}_6$ (bpy = 2,2'-bipyridine) was used as a standard ($\Phi_{\text{ref}} = 0.029$). Yields were calculated by $\Phi_x = \Phi_{\text{ref}} (\text{Grad}_x / \text{Grad}_{\text{ref}}) (\eta_x^2 / \eta_{\text{ref}}^2)$ (multiple point) or $\Phi_x = \Phi_{\text{ref}} (I_x A_{\text{ref}} / I_{\text{ref}} A_x)$ (single point), in which the subscripts ref. and x denote the reference and unknown, respectively, Φ is the fluorescence quantum yield, Grad is the gradient from the plot of integrated fluorescence intensity versus absorbance, η is the refractive index of the solvent, I is the integrated emission spectra, and A is the absorbance at a particular wavelength. Estimated uncertainty is $\pm 10\%$.

Computational methods: Density functional theory (DFT) calculations were carried out within the Gaussian09 suite of programs.^[29] Ground state geometries were optimised in the absence of solvent with B3LYP^[30] and mPW1PW91^[31] functionals in conjunction with the 6–31+G(d) basis set^[32] for non-metal atoms and the LANL2DZ basis set and core potential for platinum.^[33] Only mPW1PW91 results are presented since it has been shown previously that this functional yields reliable results.^[34] Symmetry of the optimised ground state structures is C_1 for all systems except complex 2 (C_2). Final single-point energy calculations were carried out at the 6–31+G(d)/LANL2DZ optimised geometries using the SDD basis and core potential (MWB)^[33a,35] for Pt and the TZVP basis set^[36] for all other atoms. The polarisable continuum model (PCM)^[37] self-consistent reaction field (SCRf) was used to model solvent effects at the gas-phase optimised geometries with a solvent of dichloromethane, consistent with the experimental system. HOMO and LUMO energies were calculated using DFT MOs. Excitation energies to singlet and triplet excited states were investigated with TD-DFT^[38] with 40 states calculated. An SCF convergence criteria of 10^{-8} a.u. was employed throughout. Molecular orbital analysis was carried out with the AOMix program.^[39]

Materials: All electrochemical reagents were of analytical grade or higher and were purchased from Sigma–Aldrich. Electrochemical grade TBAPF₆ electrolyte was used and organic solvents were distilled and

stored over sieved prior to use. All synthetic chemicals used in the synthesis were commercial products of reagent grade and were used without further purification.

Ligand synthesis: The Schiff base ligands were synthesised by dissolving 4,5-dimethyl-1,2-phenylenediamine (100 mg) in methanol (5 mL) and slightly more than 2 molar equivalence of the respective aldehydes in methanol (3 mL) and mixing the two. The resulting solutions were left overnight, yielding crystals of the product, which were filtered off, washed with methanol and dried in vacuo.

Salophen (a): Yield: 93%; m.p. 133°C ; ¹H NMR (200 MHz, [D₆]DMSO): $\delta = 13.17$ (s, 2H, OH), 8.62 (s, 2H, HC=N), 7.38–7.33 (m, 4H, aromatic–CH), 7.04 (d, 2H, aromatic–CH), 7.03 (s, 2H, N–CH), 6.91 (td, 2H, aromatic–CH), 2.33 ppm (s, 6H, –CH₃); EIMS: calcd for $[\text{C}_{22}\text{H}_{20}\text{N}_2\text{O}_2\text{–H}]^+$ 344.15; found: 344.1.

4,6-(OMe)₂-salophen (b): Yield: 85%; m.p. 204°C ; ¹H NMR (200 MHz, [D₆]DMSO): $\delta = 14.62$ (s, 2H, OH), 8.90 (s, 2H, HC=N), 7.03 (s, 2H, N–CH), 6.12 (d, 2H, CH–aromatic), 5.82 (d, 2H, CH–aromatic), 3.82 (s, 6H, –OCH₃), 3.80 (s, 6H, –OCH₃), 2.31 ppm (s, 6H, –CH₃); EIMS: calcd for $[\text{C}_{26}\text{H}_{28}\text{N}_2\text{O}_6\text{–H}]^+$ 464.19; found: 464.2.

4-OMe-salophen (c): Yield: 94%; m.p. 181°C ; ¹H NMR (200 MHz, [D₆]DMSO): $\delta = 13.72$ (s, 2H, OH), 8.53 (s, 2H, HC=N), 7.01 (s, 2H, N–CH), 7.24 (d, 2H, CH–aromatic), 6.54 (d, 2H, CH–aromatic), 6.45 (d, 2H, CH–aromatic), 3.83 (s, 6H, –OCH₃), 2.32 ppm (s, 6H, –CH₃); EIMS: calcd for $[\text{C}_{24}\text{H}_{24}\text{N}_2\text{O}_4\text{–H}]^+$ 404.17; found: 404.2.

6-Me-salophen (d): Yield: 97%; m.p. 196°C ; ¹H NMR (200 MHz, [D₆]DMSO): $\delta = 14.08$ (s, 2H, OH), 9.10 (s, 2H, HC=N), 7.02 (s, 2H, N–CH), 7.25 (t, 2H, CH–aromatic), 6.62 (d, 2H, CH–aromatic), 6.33 (d, 2H, CH–aromatic), 3.85 (s, 6H, –OCH₃), 2.33 ppm (s, 6H, –CH₃); EIMS: calcd for $[\text{C}_{24}\text{H}_{24}\text{N}_2\text{O}_4\text{–H}]^+$ 404.17; found: 404.2.

3-OMe-salophen (e): Yield: 76%; m.p. 158°C ; ¹H NMR (200 MHz, [D₆]DMSO): $\delta = 13.29$ (s, 2H, OH), 8.61 (s, 2H, HC=N), 7.02–6.80 (m, 8H, aromatic–CH), 3.90 (s, 6H, –OCH₃), 2.33 ppm (s, 6H, –CH₃); EIMS: calcd for $[\text{C}_{24}\text{H}_{24}\text{N}_2\text{O}_4\text{–H}]^+$ 404.17; found: 404.2.

5-OMe-salophen (f): Yield: 92%; m.p. 128°C ; ¹H NMR (200 MHz, [D₆]DMSO): $\delta = 12.68$ (s, 2H, OH), 8.59 (s, 2H, HC=N), 7.03 (s, 2H, N–CH), 3.79 (s, 6H, –OCH₃), 2.33 ppm (s, 6H, –CH₃); EIMS: calcd for $[\text{C}_{24}\text{H}_{24}\text{N}_2\text{O}_4\text{–H}]^+$ 404.17; found: 404.2.

3,5-(OMe)₂-salophen (g): Yield: 87%; m.p. 84°C ; ¹H NMR (200 MHz, [D₆]DMSO): $\delta = 12.84$ (s, 2H, OH), 8.56 (s, 2H, HC=N), 6.98 (s, 2H, HC=N), 6.61 (d, 2H, aromatic–CH), 6.46 (d, 2H, aromatic–CH), 3.87 (s, 6H, –OCH₃), 3.79 (s, 6H, –OCH₃), 2.34 ppm (s, 6H, –CH₃); EIMS: calcd for $[\text{C}_{26}\text{H}_{28}\text{N}_2\text{O}_6\text{–H}]^+$ 464.19; found: 464.1.

Complex synthesis

[Pt-salophen] (1): K₂PtCl₄ (0.0688 g) was added to an 80°C mixture of the ligand Salophen (0.0524 g) and sodium acetate (0.0274 g) in DMSO (4 mL). The mixture was heated to 110°C for 3 h with stirring. The reaction mixture was then cooled to room temperature. Small red crystals of product were filtered off and washed with DMSO (2 mL), methanol (4 mL) and ether (8 mL). The product was then dried, overnight at 100°C . Yield: 0.0719 g (85%); m.p. $> 320^\circ \text{C}$; ¹H NMR (200 MHz, [D₆]DMSO): $\delta = 9.38$ (s, 2H, HC=N, (with Pt satellites)), 8.18 (s, 2H, N–C–CH), 7.80 (dd, 2H, CH–aromatic), 7.53 (dt, 2H, CH–aromatic), 7.07 (d, 2H, CH–aromatic), 6.75 (t, 2H, CH–aromatic), 2.32 ppm (s, 6H, –CH₃); HRMS (ESI): m/z calcd for $[\text{C}_{22}\text{H}_{18}\text{N}_2\text{O}_2\text{Pt–H}]^+$ 537.1073; found: 537.1056; elemental analysis calcd (%) for C₂₂H₁₈N₂O₂Pt: C 49.16, H 3.38, N 5.21; found: C 49.03, H 3.53, N 5.12.

[Pt-4,6-(OMe)₂-salophen] (2): K₂PtCl₄ (0.0487 g) was added to an 80°C mixture of the ligand 4,6-(OMe)₂-Salophen (0.0508 g) and sodium acetate (0.0260 g) in DMSO (4 mL). The mixture was heated to 110°C for 3 h with stirring. The reaction mixture was then cooled to room temperature. Some small crystals had formed. Water (4 mL) was added to precipitate the remainder of the platinum complex. The product was filtered off and washed with 50% aqueous DMSO (1 mL), methanol (4 × 1 mL) and ether (4 × 2 mL). The product was then dried at 100°C . Yield: 0.0545 g (76%); m.p. $> 320^\circ \text{C}$; ¹H NMR (200 MHz, [D₆]DMSO): $\delta = 9.23$ (s, 2H, HC=N, (with Pt satellites)), 7.89 (s, 2H, N–C–CH), 6.21 (d, 2H, CH–aromatic), 5.94 (d, 2H, CH–aromatic), 3.90 (s, 6H, –OCH₃), 3.80 (s, 6H, –

OCH₃), 2.32 ppm (s, 6H, -CH₃); HRMS (ESI): *m/z* calcd for [C₂₆H₂₆N₂O₆Pt-Na]⁺ 679.1315; found: 679.1329; elemental analysis calcd (%) for C₂₆H₂₆N₂O₆Pt: C 47.49, H 3.99, N 4.26; found: C 47.73, H 4.05, N 4.32.

[Pt-4-Ome-salophen] (3): K₂PtCl₄ (0.0538 g) was added to an 80 °C mixture of the ligand 4-(OMe)-Salophen (0.0504 g) and sodium acetate (0.0233 g) in DMSO (4 mL). The mixture was heated to 110 °C for 3 h with stirring. The reaction mixture was then cooled to room temperature. Small red crystals of product were filtered off and washed with methanol (4 mL) and ether (8 mL). The product was then dried, overnight, at 100 °C. Yield: 0.0555 g (75 %); m.p. >320 °C; ¹H NMR (200 MHz, [D₆]DMSO): δ=9.19 (s, 2H, HC=N, (with Pt satellites)), 8.11 (s, 2H, N-C-CH), 7.68 (d, 2H, CH-aromatic), 6.57 (d, 2H, CH-aromatic), 6.44 (dd, 2H, CH-aromatic), 3.81 (s, 6H, -OCH₃), 2.33 ppm (s, 6H, -CH₃); HRMS (ESI): *m/z* calcd for [C₂₄H₂₂N₂O₄Pt-Na]⁺ 619.1104; found: 619.1115; elemental analysis calcd (%) for C₂₄H₂₂N₂O₄Pt: C 48.24, H 3.71, N 4.69; found: C 48.46, H 3.77, N 4.83.

[Pt-6-Ome-salophen] (4): K₂PtCl₄ (0.0538 g) was added to an 80 °C mixture of the ligand 6-(OMe)-Salophen (0.0507 g) and sodium acetate (0.0238 g) in DMSO (4 mL). The mixture was heated to 110 °C for 3 h with stirring. The reaction mixture was then cooled to room temperature. Small red crystals of product were filtered off and washed with DMSO (2 mL), 50 % aqueous DMSO (2 mL), methanol (4 mL) and ether (8 mL). The product was then dried, overnight, at 100 °C. Yield: 0.0485 g (65 %); m.p. >320 °C; ¹H NMR (200 MHz, [D₆]DMSO): δ=9.51 (s, 2H, HC=N, (with Pt satellites)), 7.99 (s, 2H, N-C-CH), 7.39 (t, 2H, CH-aromatic), 6.69 (d, 2H, CH-aromatic), 6.32 (d, 2H, CH-aromatic), 3.93 (s, 6H, -OCH₃), 2.35 ppm (s, 6H, -CH₃); HRMS (ESI): *m/z* calcd for [C₂₄H₂₂N₂O₄Pt-H]⁺ 597.1227; found: 597.1229; elemental analysis calcd (%) for C₂₄H₂₂N₂O₄Pt: C 48.24, H 3.71, N 4.69; found: C 48.42, H 3.79, N 4.78.

[Pt-3-Ome-salophen] (5): K₂PtCl₄ (0.0540 g) was added to an 80 °C mixture of the ligand 3-(OMe)-Salophen (0.0516 g) and sodium acetate (0.0250 g) in DMSO (4 mL). The mixture was heated to 110 °C for 3 h with stirring. The reaction mixture was then cooled to room temperature. Small red crystals of product were filtered off and washed with DMSO (2 mL), 50 % aqueous DMSO (2 mL), methanol (4 mL) and ether (8 mL). The product was then dried, overnight, at 100 °C. Yield: 0.0633 g (83 %); m.p. >320 °C; ¹H NMR (200 MHz, [D₆]DMSO): δ=9.37 (s, 2H, HC=N, (with Pt satellites)), 8.22 (s, 2H, N-C-CH), 7.40 (dd, 2H, CH-aromatic), 7.12 (dd, 2H, CH-aromatic), 6.68 (t, 2H, CH-aromatic), 3.82 (s, 6H, -OCH₃), 2.35 ppm (s, 6H, -CH₃); HRMS (ESI): *m/z* calcd for [C₂₄H₂₂N₂O₄Pt-H]⁺ 597.1227; found: 597.1222; elemental analysis calcd (%) for C₂₄H₂₂N₂O₄Pt.3H₂O: C 44.24, H 4.33, N 4.30; found: C 44.29, H 3.85, N 4.30.

[Pt-5-Ome-salophen] (6): K₂PtCl₄ (0.0530 g) was added to an 80 °C mixture of the ligand 5-(OMe)-Salophen (0.0500 g) and sodium acetate (0.0231 g) in DMSO (4 mL). The mixture was heated to 110 °C for 12 h with stirring. The resulting dark red solution was cooled to room temperature. Water (1 mL) was added precipitating out the product. The product was filtered and washed with methanol (4 mL) and ether (8 mL). The product was then dried, overnight, at 100 °C. Yield: 0.0604 g (68 %); m.p. >320 °C; ¹H NMR (200 MHz, [D₆]DMSO): δ=9.31 (s, 2H, HC=N), 8.11 (s, 2H, N-C-CH), 7.27 (d, 2H, CH-aromatic), 7.23 (dd, 2H, CH-aromatic), 7.02 (d, 2H, CH-aromatic), 3.75 (s, 6H, -OCH₃), 2.29 ppm (s, 6H, -CH₃); HRMS (ESI): *m/z* calcd for [C₂₄H₂₂N₂O₄Pt-Na]⁺ 619.1104; found: 619.1091; elemental analysis calcd (%) for C₂₄H₂₂N₂O₄Pt: C 48.24, H 3.71, N 4.69; found: C 48.38, H 4.04, N 4.52.

[Pt-3,5-(OMe)₂-salophen] (7): K₂PtCl₄ (0.0493 g) was added to an 80 °C mixture of the ligand 3,5-(OMe)₂-salophen (0.0506 g) and sodium acetate (0.0260 g) in DMSO (4 mL). The mixture was heated to 110 °C for 3 h with stirring. The reaction mixture was then cooled to room temperature. Small red crystals of product were filtered off and washed with DMSO (4 mL), methanol (5 mL) and ether (8 mL). The product was then dried, overnight, at 100 °C. Yield: 0.0525 g (81 %); m.p. >320 °C; ¹H NMR (200 MHz, [D₆]DMSO): δ=9.29 (s, 2H, HC=N, (with Pt satellites)), 8.14 (s, 2H, N-C-CH), 6.83 (d, 2H, CH-aromatic), 6.78 (d, 2H, CH-aromatic), 3.81 (s, 6H, -OCH₃), 3.76 (s, 6H, -OCH₃), 2.32 ppm (s, 6H, -CH₃);

HRMS (ESI): *m/z* calcd for [C₂₆H₂₆N₂O₆Pt-H]⁺ 657.1439; found: 657.1435; elemental analysis calcd (%) for C₂₆H₂₆N₂O₆Pt: C 47.49, H 3.99, N 4.26; found: C 46.91, H 4.01, N 4.18.

Acknowledgements

C.F.H. acknowledges the Australian Research Council (ARC) for a discovery project grant (DP1094179). The authors acknowledge support from the National Computational Infrastructure National Facility (NCINF), Victorian Partnership for Advanced Computing (VPAC), Victorian Life Science Computing Initiative (VLSICI) and the high performance computing facility of La Trobe University.

- a) J. A. Williams, A. J. Wilkinson, V. J. Whittle, *Dalton Trans.* **2008**, 2081–2099; b) S. Huo, J. C. Deaton, M. Rajeswaran, W. C. Lenhart, *Inorg. Chem.* **2006**, *45*, 3155–3157; c) C.-L. Lee, N.-G. Kang, Y.-S. Cho, J.-S. Lee, J.-J. Kim, *Opt. Mater.* **2003**, *21*, 119–123; d) C. Ulbricht, B. Beyer, C. Friebe, A. Winter, U. S. Schubert, *Adv. Mater.* **2009**, *21*, 4418–4441.
- a) F. Matar, T. H. Ghaddar, K. Walley, T. DosSantos, J. R. Durrant, B. O'Regan, *Mater. Chem.* **2008**, *18*, 4246–4253; b) J.-J. Kim, H. Choi, C. Kim, M.-S. Kang, H. S. Kang, J. Ko, *Chem. Mater.* **2009**, *21*, 5719–5726; c) C.-Y. Chen, N. Pootrakulchote, S.-J. Wu, M. Wang, J.-Y. Li, J. H. Tsai, C.-G. Wu, S. M. Zakeeruddin, M. Gratzel, *J. Phys. Chem. C* **2009**, *113*, 20752–20757.
- a) C. Huo, H. Zhang, H. Zhang, H. Zhang, B. Yang, P. Zhang, Y. Wang, *Inorg. Chem.* **2006**, *45*, 4735–4742; b) H. Zhang, Y. Sun, K. Ye, P. Zhang, Y. Wang, *J. Mater. Chem.* **2005**, *15*, 3181–3186; c) A. S. Holmes-Smith, A. Hamill, M. Campbell, M. Uttamlal, *Analyst* **1999**, *124*, 1463–1466.
- a) T. Abe, T. Itakura, N. Ikeda, K. Shinozaki, *Dalton Trans.* **2009**, 711–715; b) S. C. F. Kui, I. H. T. Sham, C. C. C. Cheung, C.-W. Ma, B. Yan, N. Zhu, C.-M. Che, W.-F. Fu, *Chem. Eur. J.* **2007**, *13*, 417–435; c) K. M.-C. Wong, V. W.-W. Yam, *Coord. Chem. Rev.* **2007**, *251*, 2477–2488; d) K. M.-C. Wong, W.-S. Tang, X.-X. Lu, N. Zhu, V. W.-W. Yam, *Inorg. Chem.* **2005**, *44*, 1492–1498.
- L. Ancarani Rossiello, *J. Chem. Phys.* **1969**, *51*, 5191–5192.
- J. A. Miller, W. Jin, S. T. Nguyen, *Angew. Chem.* **2002**, *117*, 3953–3957; *Angew. Chem. Int. Ed.* **2002**, *41*, 2953–2956.
- R. L. Paddock, S. T. Nguyen, *J. Am. Chem. Soc.* **2001**, *123*, 11498–11499.
- G. A. Morris, H. Zhou, C. L. Stern, S. Y. Nguyen, *Inorg. Chem.* **2001**, *40*, 3222–3227.
- W.-L. Tong, L.-M. Lai, M. C. Chan, *Dalton Trans.* **2008**, 1412–1414.
- a) M. E. Ivanova, G. A. Shagisultanova, *Russ. J. Phys. Chem. A* **1991**, *65*, 1563; b) G. A. Shagisultanova, I. E. Popenko, A. M. Timonov, *Russ. J. Inorg. Chem.* **1991**, *36*, 3096.
- a) Y.-Y. Lin, S.-C. Chan, M. C. W. Chan, Y.-J. Hou, N. Zhu, C.-M. Che, Y. Liu, Y. Wang, *Chem. Eur. J.* **2003**, *9*, 1263–1272; b) C.-M. Che, S.-C. Chan, H.-F. Xiang, M. C. W. Chan, Y. Liu, Y. Wang, *Chem. Commun.* **2004**, 1484–1485; c) C.-M. Che, C.-C. Kwok, S.-W. Lai, A. F. Rausch, W. J. Finkenzeller, N. Zhu, H. Yersin, *Chem. Eur. J.* **2010**, *16*, 233–247.
- a) E. H. Doeven, E. M. Zammit, G. J. Barbante, P. S. Francis, N. W. Barnett, C. F. Hogan, *Chem. Sci.* **2013**, *4*, 977–982; b) T. Joshi, G. J. Barbante, P. S. Francis, C. F. Hogan, A. M. Bond, G. Gasser, L. Spiccia, *Inorg. Chem.* **2012**, *51*, 3302–3315; c) E. H. Doeven, E. M. Zammit, G. J. Barbante, C. F. Hogan, N. W. Barnett, P. S. Francis, *Angew. Chem.* **2012**, *124*, 4430–4433; *Angew. Chem. Int. Ed.* **2012**, *51*, 4354–4357; d) T. Joshi, G. J. Barbante, P. S. Francis, C. F. Hogan, A. M. Bond, L. Spiccia, *Inorg. Chem.* **2011**, *50*, 12172–12183; e) J. L. Adcock, C. J. Barrow, N. W. Barnett, X. A. Conlan, C. F. Hogan, P. S. Francis, *Drug Test. Anal.* **2011**, *3*, 145–160.
- G. J. Barbante, C. F. Hogan, A. Mechler, A. B. Hughes, *J. Mater. Chem.* **2010**, *20*, 891–899.

- [14] a) T. R. Long, M. M. Richter, *Inorg. Chim. Acta* **2005**, *358*, 2141–2145; b) P. Canty, L. Väre, M. Håkansson, A. M. Spehar, D. Papkovsky, T. Ala-Kleme, J. Kankare, S. Kulmala, *Anal. Chim. Acta* **2002**, *453*, 269–279; c) S. Bonafede, M. Ciano, F. Bolletta, V. Balzani, L. Chassot, A. Von Zelewsky, *J. Phys. Chem.* **1986**, *90*, 3836–3841; d) N. A. P. Kane-Maguire, L. L. Wright, J. A. Guckert, W. S. Tweet, *Inorg. Chem.* **1988**, *27*, 2905–2907; e) J. Kim, F. F. Fan, A. J. Bard, C.-M. Che, H. B. Gray, *Chem. Phys. Lett.* **1985**, *121*, 543–546; f) N. E. Tokel-Takvoryan, A. J. Bard, *Chem. Phys. Lett.* **1974**, *25*, 235–238.
- [15] X. Q. Lü, W. Y. Wong, W. K. Wong, *Eur. J. Inorg. Chem.* **2008**, 523–528.
- [16] D. Babic, M. Curic, K. Molcanov, G. Ilc, J. Plavec, *Inorg. Chem.* **2008**, *47*, 10446–10454.
- [17] Z.-X. Liao, Y. Wang, X.-P. Yang, Z. D. Zhou, D. Xiao, *Chem. Phys. Lett.* **2007**, *440*, 329–333.
- [18] G. J. Barbante, C. F. Hogan, D. J. D. Wilson, N. A. Lewcenko, F. M. Pfeffer, N. W. Barnett, P. S. Francis, *Analyst* **2011**, *136*, 1329–1338.
- [19] A. Kapturkiewicz, P. Szrebrowaty, G. Angulo, G. Grampp, *J. Phys. Chem. A* **2002**, *106*, 1678–1685.
- [20] a) I.-S. Shin, J. I. Kim, T.-H. Kwon, J.-I. Hong, J.-K. Lee, H. Kim, *J. Phys. Chem. C* **2007**, *111*, 2280–2286; b) N. E. Tokel, A. J. Bard, *J. Am. Chem. Soc.* **1972**, *94*, 2862–2863.
- [21] Our reasoning here is that the formation of the Pt^{II} excited state from the reaction in Equation (3) would require the reduced partner to become the excited product. The electron transfer between two substantially metal based orbitals that this involves is far less likely, from an orbital overlap point of view, than the ligand-to-ligand electron transfer required in the reaction in Equation (4).
- [22] R. J. Forster, P. Bertoncello, T. E. Keyes, *Ann. Rev. Anal. Chem.* **2009**, *2*, 359–385.
- [23] R. A. Marcus, *J. Chem. Phys.* **1956**, *24*, 966–978.
- [24] Inhibition of the rate of the annihilation reaction leading to the ground state product is predicted by Marcus theory for larger values of $-\Delta G_{\text{ann}}$.
- [25] A. J. Bard, *Electrogenerated Chemiluminescence*, CRC, Boca Raton, **2004**.
- [26] J. Kim, I. Shin, H. Kim, J. Lee, *J. Am. Chem. Soc.* **2005**, *127*, 1614–1615.
- [27] W. Miao, J.-P. Choi, A. J. Bard, *J. Am. Chem. Soc.* **2002**, *124*, 14478–14485.
- [28] a) Q. Zhao, S. Liu, M. Shi, C. Wang, M. Yu, L. Li, F. Li, T. Yi, C. Huang, *Inorg. Chem.* **2006**, *45*, 6152–6160; b) M. Zhou, G. P. Robertson, J. Roovers, *Inorg. Chem.* **2005**, *44*, 8317–8325.
- [29] Gaussian 09, Revision A 0.2, M. J. Frisch, G. W. Trucks, H. B. Schlegel, G. E. Scuseria, M. A. Robb, J. R. Cheeseman, G. Scalmani, V. Barone, B. Mennucci, G. A. Petersson, H. Nakatsuji, M. Caricato, X. Li, H. P. Hratchian, A. F. Izmaylov, J. Bloino, G. Zheng, J. L. Sonnenberg, M. Hada, M. Ehara, K. Toyota, R. Fukuda, J. Hasegawa, M. Ishida, T. Nakajima, Y. Honda, O. Kitao, H. Nakai, T. Vreven, J. A. Montgomery, J. E. Peralta, F. Ogliaro, M. Bearpark, J. J. Heyd, E. Brothers, K. N. Kudin, V. N. Staroverov, R. Kobayashi, J. Normand, K. Raghavachari, A. Rendell, J. C. Burant, S. S. Iyengar, J. Tomasi, M. Cossi, N. Rega, J. M. Millam, M. Klene, J. E. Knox, J. B. Cross, V. Bakken, C. Adamo, J. Jaramillo, R. Gomperts, R. E. Stratmann, O. Yazyev, A. J. Austin, R. Cammi, C. Pomelli, J. W. Ochterski, R. L. Martin, K. Morokuma, V. G. Zakrzewski, G. A. Voth, P. Salvador, J. J. Dannenberg, S. Dapprich, A. D. Daniels, Ö. Farkas, J. B. Foresman, J. V. Ortiz, J. Cioslowski, D. J. Fox, Gaussian, Inc., Wallingford CT, **2009**.
- [30] a) A. D. Becke, *Phys. Rev. A* **1988**, *38*, 3098–3100; b) A. D. Becke, *J. Chem. Phys.* **1993**, *98*, 5648–5652; c) C. Lee, W. Yang, R. G. Parr, *Phys. Rev. B* **1988**, *37*, 785–789.
- [31] a) C. Adamo, V. Barone, *J. Chem. Phys.* **1998**, *108*, 664–675; b) J. P. Perdew, in *Electronic Structure of Solids* (Eds.: P. Ziesche, H. Eschrig), Akademie, Berlin, **1991**, pp. 11–20.
- [32] a) W. J. Hehre, R. Ditchfield, J. A. Pople, *J. Chem. Phys.* **1972**, *56*, 2257–2261; b) P. C. Hariharan, J. A. Pople, *Theor. Chim. Acta* **1973**, *28*, 213–222; c) T. Clark, J. Chandrasekhar, G. W. Spitznagel, P. v. R. Schleyer, *J. Comput. Chem.* **1983**, *4*, 294–301.
- [33] a) T. H. Dunning, Jr., P. J. Hay, in *Modern Theoretical Chemistry, Vol. 3* (Ed.: H. F. Schaefer III), Plenum, New York, **1976**, pp. 1–28; b) P. J. Hay, W. R. Wadt, *J. Chem. Phys.* **1985**, *82*, 270–283.
- [34] J. Lin, K. Wu, M. Zhang, *J. Comput. Chem.* **2009**, *30*, 2056–2063.
- [35] D. Andrae, U. Haeussermann, M. Dolg, H. Stoll, H. Preuss, *Theor. Chim. Acta* **1990**, *77*, 123–141.
- [36] A. Schäfer, H. Horn, R. Ahlrichs, *J. Chem. Phys.* **1992**, *97*, 2571–2517.
- [37] J. Tomasi, B. Mennucci, R. Cammi, *Chem. Rev.* **2005**, *105*, 2999–3093.
- [38] R. E. Stratmann, G. E. Scuseria, M. J. Frisch, *J. Chem. Phys.* **1998**, *109*, 8218–8224.
- [39] S. I. Gorelsky, AOMix: Program for Molecular Orbital Analysis, Version 6.46, University of Ottawa: <http://www.sg-chem.net/>, **2010**.

Received: June 19, 2013
Published online: October 2, 2013